Implementation of the Reynolds-stress Turbulence Model

Patrik Rautaheimo and **Timo Siikonen** [1]

Abstract. The implementation of the Reynolds-stress model in a multi-block Navier-Stokes solver is described. The inviscid part of the flux is calculated using Roe's method. Two methods have been developed in order to couple the Reynolds-stress equations and the flow equations. For the calculation of the inviscid and Reynolds-stress parts of the flux, the Cartesian form is used by applying a suitable rotation operator. A similar operator is applied for an easy calculation of the symmetry boundary condition. The flow equations are solved implicitly using a multigrid acceleration for convergence. The algorithm is applied for flows in a plane and in a curved channel with fairly good results. In the calculated cases the convergence is fast.

1 INTRODUCTION

In recent years, many developments have been made in order to couple the Reynolds-averaged Navier–Stokes equations (RANS) and turbulence models. With algebraic models numerical methods remain essentially the same as in a laminar case, but the implementation of the Reynolds-stress turbulence model in the curvilinear coordinate system is a difficult task, see e.g. [11]. The difficulties include the robustness and efficiency of the numerical scheme as well as the complexity of the computer code. This complexity may cause coding errors and also reduce the efficiency.

In this paper the implementation of the Reynolds-stress model in an existing multi-block Navier-Stokes solver [20] is described. In order to minimize the coding errors, a Cartesian form of the fluxes is utilized for the inviscid terms and for the Reynolds stresses. This is accomplished by applying suitable rotating operators. The flow equations are solved using Roe's flux-difference splitting. The solution is based on the time integration. In incompressible flow cases a pseudocompressibility approach [4] with a Roe-type damping term can be applied. In order to increase the robustness of the method, the flow equations and the Reynolds-stress equations are coupled in the approximate Riemann solution. Two coupling methods between the RANS equations and the equations for the Reynolds stresses have been developed [16].

[1] Laboratory of Applied Thermodynamics, Helsinki University of Technology, 02150 Espoo, Finland

Computational Fluid Dynamics '96
Published in 1996 by John Wiley & Sons, Ltd.

In the following the Reynolds-stress model and its implementation are briefly described. The algorithm is applied for a flow in a plane channel [8] and for a flow in a curved duct [9].

2 GOVERNING EQUATIONS

2.1 Reynolds-Stress Model

The flow simulation is based on the solution of the Reynolds averaged Navier–Stokes equations:

$$\frac{\partial U}{\partial t} + \frac{\partial (F - F_v)}{\partial x} + \frac{\partial (G - G_v)}{\partial y} + \frac{\partial (H - H_v)}{\partial z} = Q \quad (1)$$

where U is the vector of dependent variables, F, G, H and F_v, G_v, H_v represent the inviscid and viscous parts of the fluxes, and Q is a possible source term.

The Reynolds-stress model (RSM) can be written in the following form

$$\frac{\partial \bar{\rho} \widetilde{u_i'' u_j''}}{\partial t} + \frac{\partial (\bar{\rho} \bar{u}_k \widetilde{u_i'' u_j''})}{\partial x_k} = P_{ij} + \Phi_{ij} + D_{ij} - \epsilon_{ij} \quad (2)$$

where $P_{ij}, \Phi_{ij}, D_{ij}$ and ϵ_{ij} are the production term, the pressure-strain term, the diffusion term and the dissipation term, respectively.

The production term is exact, whereas the turbulent diffusion, the pressure strain and the dissipation rate must be modeled. In this work two different high-Reynolds number models are applied, one developed by Launder, Reece and Rodi (hereafter referred as LRR) [10] and the other by Speziale, Sarkar and Gatski (hereafter referred as SSG) [21]. The low-Reynolds number modeling is based on Shima's work [18]. In the SSG model the low-Reynolds number model is adapted from Shima in a similar way as in [2]. In both cases the dissipation transport equation is based on Chien's $k - \epsilon$ model [3].

In Shima's low-Reynolds number model the pressure-strain and the dissipation rate terms are connected as

$$\overline{p' \left(\frac{\partial u_i''}{\partial x_j} + \frac{\partial u_j''}{\partial x_i} \right)} - 2\mu \overline{\frac{\partial u_i''}{\partial x_k} \frac{\partial u_j''}{\partial x_k}} = \Phi_{ij} - \epsilon_{ij} =$$

$$\phi_{ij,1} + \phi_{ij,2} + \phi_{ij,w} - \frac{2}{3}\delta_{ij}\bar{\rho}\epsilon \qquad (3)$$

where $\phi_{ij,1}$ represents the fluctuation part of Φ_{ij} and ϵ_{ij}, $\phi_{ij,2}$ the mean-strain part of Φ_{ij}, and $\phi_{ij,w}$ takes into account the wall proximity effects. These terms can be written in the following way [21]

$$\begin{aligned}\phi_{ij,1} &= -\left[\bar{C}_1 - (\bar{C}_1 - 2)f_w\right]\epsilon\, b_{ij} \\ &\quad + C_2\,(1 - f_w)\,\epsilon\,(b_{ik}\,b_{kj} - \frac{1}{3}\Pi\delta_{ij}) \qquad (4)\\ \phi_{ij,2} &= (C_3 - C_3^*\Pi^{1/2})\bar{\rho}\,k\,S_{ij} + \\ &\quad C_4\,\bar{\rho}k(b_{ik}\,S_{jk} + b_{jk}\,S_{ik} - \frac{2}{3}b_{kl}\,S_{kl}\delta_{ij}) + \\ &\quad C_5\,\bar{\rho}k(b_{ik}\,W_{jk} + b_{jk}\,W_{ik}) \qquad (5)\\ \phi_{ij,w} &= [\alpha\left(P_{ij} - \frac{2}{3}\delta_{ij}P\right) + \gamma\bar{\rho}kS_{ij} + \\ &\quad \beta\left(D_{ij} - \frac{2}{3}\delta_{ij}P\right)]f_w \qquad (6)\end{aligned}$$

where P_{ij}, D_{ij} and P are

$$\begin{aligned}P_{ij} &= -\left[\bar{\rho}\widetilde{u_i''u_k''}\frac{\partial\tilde{u}_j}{\partial x_k} + \bar{\rho}\widetilde{u_j''u_k''}\frac{\partial\tilde{u}_i}{\partial x_k}\right] \qquad (7)\\ D_{ij} &= -\left[\bar{\rho}\widetilde{u_i''u_k''}\frac{\partial\tilde{u}_k}{\partial x_j} + \bar{\rho}\widetilde{u_j''u_k''}\frac{\partial\tilde{u}_k}{\partial x_i}\right] \qquad (8)\\ P &= -\bar{\rho}\widetilde{u_k''u_l''}\frac{\partial\tilde{u}_k}{\partial x_l} \qquad (9)\\ f_w &= \exp\left[-\left(0.015\frac{\rho\sqrt{k}y_n}{\mu}\right)^4\right] \qquad (10)\end{aligned}$$

and

$$\begin{aligned}b_{ij} &= \frac{\widetilde{u_i''u_j''}}{2k} - \frac{1}{3}\delta_{ij} \qquad \Pi = b_{kl}b_{kl}\\ S_{ij} &= \frac{1}{2}\left(\frac{\partial\tilde{u}_i}{\partial x_j} + \frac{\partial\tilde{u}_j}{\partial x_i}\right) \qquad W_{ij} = \frac{1}{2}\left(\frac{\partial\tilde{u}_i}{\partial x_j} - \frac{\partial\tilde{u}_j}{\partial x_i}\right)\\ \bar{C}_1 &= C_1 + C_1^*P/\epsilon \qquad (11)\end{aligned}$$

The multiplyer in the exponent of Eq.(10) was, after test calculations, modified to be 0.013. It should also be noted that in this study when Shima's model was used the tangential components of the wall term $\phi_{ij,w}$ were omitted in order to get a correct velocity profile and shear-stress distribution close to the wall.

Table 1. Constants in the pressure-strain term.

Model	C_1	C_1^*	C_2	C_3	C_3^*	C_4	C_5
Shima	3.0	0.0	0.0	0.8	0.0	1.75	1.31
SSG	3.4	1.84	4.2	0.8	1.30	1.25	0.40

Eqs. (4) -(6) are written in a general form. Different models can be written by changing the constants. The applied constants are presented in Table 1.

The wall correction term includes parameters α, β and γ, which also have different values. The values for Shima's model are from [18], and the values for the SSG model were assigned after test calculations.

Table 2. Constants in the wall correction term.

Model	α	β	γ
Shima	0.45	0.0	0.08
SSG	0.23	0.125	0.085

In this work diffusion is calculated using a simple scalar diffusion [6]

$$D_{ij} = \frac{\partial}{\partial x_k}\left[\left(\mu + \mu_T/\sigma_{ij,T}\right)\frac{\partial\widetilde{u_i''u_j''}}{\partial x_k}\right] \qquad (12)$$

where the turbulent eddy viscosity μ_T is defined as

$$\mu_T = c_\mu\bar{\rho}\frac{k^2}{\epsilon} \qquad (13)$$

and $\sigma_{ij,T}$=1.0 Also the model of Daly and Harlow [5]

$$\overline{\rho u_i''u_j''u_k''} + \delta_{ik}\overline{p'u_j''} + \delta_{jk}\overline{p'u_i''} = -c_s'\frac{k}{\epsilon}\bar{\rho}\widetilde{u_k''u_l''}\frac{\partial}{\partial x_l}\widetilde{u_i''u_j''} \qquad (14)$$

was tested, but it did not give any improvement over Eq. (12).

2.2 Dissipation Transport Equation

The dissipation transport equation is adopted from Chien's $k-\epsilon$ model [3] because it was experienced to be stable and well behaved. Chien's dissipation transport equation can be written as

$$\bar{\rho}\frac{D\hat{\epsilon}}{Dt} = \frac{\partial}{\partial x_i}\left[(\mu + \mu_T/\sigma_\epsilon)\frac{\partial\hat{\epsilon}}{\partial x_j}\right] + c_1\frac{\hat{\epsilon}}{k}P - c_2\frac{\bar{\rho}\hat{\epsilon}^2}{k} - 2\mu\frac{\hat{\epsilon}}{y_n^2}e^{-y^+/2} \qquad (15)$$

where y_n is the normal distance from the wall, and y^+ is defined by

$$y^+ = y_n\frac{\rho u_\tau}{\mu} = y_n\frac{\sqrt{\rho\tau_w}}{\mu} = y_n\left[\frac{\rho|\nabla\times\vec{V}|}{\mu}\right]_w^{1/2} \qquad (16)$$

The relationship between ϵ and $\hat{\epsilon}$ is

$$\epsilon = \hat{\epsilon} + D \qquad (17)$$

$$D = 2\nu\frac{k}{y_n^2} \qquad (18)$$

where ν is kinematic viscosity. With this assumption, $\hat{\epsilon}$ has a value of zero at the wall and ϵ has an exact value with respect to k. However, $\hat{\epsilon}$ does not have the desired $O(y^2)$ behaviour near the wall. This results in a non-zero diffusion flux at the wall.

The equation for ϵ contains empirical coefficients. The following values are applied

$$c_1 = 1.44 \quad c_2 = 1.92(1-0.22e^{-Re_T^2/36}) \qquad \sigma_\epsilon = 1.3 \tag{19}$$

where the turbulence Reynolds number is defined as

$$Re_T = \frac{\bar{\rho}k^2}{\mu\hat{\epsilon}} \tag{20}$$

3 NUMERICAL METHODS

The finite-volume CFD program [20] was used in the present calculations. The program utilizes Cartesian velocity components in a cell-centred approach. In the evaluation of the inviscid fluxes, Roe's method [17] is applied. For a spatial discretization a MUSCL-type TVD-scheme to approximate inviscid volume-face fluxes is applied. The discretized equations are integrated in time by applying the *DDADI*-factorization [12]. The code utilizes a multigrid V-cycle for the acceleration of convergence. Complicated geometries are handled with multiblock grids. Incompressible flows can be solved using the pseudocompressibility approach [4].

3.1 Spatial Discretization

In the present solution, a finite-volume technique is applied. The flow equations have an integral form

$$\frac{d}{dt}\int_V U\,dV + \int_S \vec{F}(U)\cdot d\vec{S} = \int_V Q\,dV \tag{21}$$

for an arbitrary fixed region V with a boundary S. Performing the integrations for a computational cell i yields

$$V_i\frac{dU_i}{dt} = -\sum_{\text{faces}} S\hat{F} + V_iQ_i \tag{22}$$

where the sum is taken over the faces of the computational cell. The flux for the face is defined as

$$\hat{F} = n_xF + n_yG + n_zH \tag{23}$$

Here F, G and H are the inviscid fluxes in the x, y and z directions, respectively.

In order to simplify coding the fluxes on the cell faces are calculated as

$$\hat{F} = \mathcal{T}^{-1}F(\mathcal{T}U) \tag{24}$$

Here U is the vector of dependent variables obtained on the cell surface using a MUSCL-type extrapolation with a second- or third-order accuracy. The rotation operator $\mathcal{T}$ transforms the dependent variables into a local coordinate system normal to the cell surface. In this way, only the Cartesian form F of the flux is needed. Velocity components are rotated from the global to the local coordinate system as

$$\begin{pmatrix}\hat{u}\\ \hat{v}\\ \hat{w}\end{pmatrix} = T\begin{pmatrix}u\\ v\\ w\end{pmatrix} \tag{25}$$

where the hats refer to the local Cartesian coordinate system. Matrix T is the rotation matrix that is determined by the normal and the tangent vectors of the cell face.

Correspondingly, the Reynolds stresses, if needed, are rotated from the global to the local coordinate system by the following formula

$$\hat{I} = TIT^T \tag{26}$$

where the components of the matrix I are the Reynolds stresses. Transformation from the local back to the global coordinate system is given by

$$I = T^T\hat{I}T \tag{27}$$

3.2 Diagonalization of the Flow Equations

The calculation of fluxes is done using Roe's approximate Riemann solver [17]. This approach is utilized also for incompressible flows. The approximate Riemann solution requires that the Jacobian matrix of the flux vector

$$A = \frac{\partial F}{\partial U} \tag{28}$$

can be put into a diagonal form, i.e. A has a complete set of eigenvectors.

As the Reynolds-stress model is applied, there is a coupling between the main flow variables and turbulence quantities, since the Reynolds stresses may be connected with the pressure [22]. In the i-momentum equation, the resulting effective pressure can be defined as

$$p_i^* = \bar{p} + \bar{\rho}\widetilde{u_i''u_i''} \tag{29}$$

Unfortunately, linearly independent eigenvectors cannot be found for the matrix A if an unisotropic pressure field of Eq. (29) is applied. In the case of a $k-\epsilon$ model with an isotropic pressure field, linearly independent eigenvectors exist [19]. Since the anisotropic pressure field is difficult to handle, the turbulent pressure can be approximated by the mean of three components

$$p^* = \bar{p} + \frac{2}{3}\bar{\rho}k \tag{30}$$

In the previous paper [16] we presented two alternatives for the diagonalization of A. In the calculated cases these methods have produced nearly identical results. The first possibility is to divide the flux-vector F into two parts

$$F = F_1 + F_2 \tag{31}$$

where F_1 corresponds to the isotropic part of the turbulence quantities and F_2 contains the anisotropic part as

$$F_1 = \begin{pmatrix} \bar{\rho}\tilde{u} \\ \bar{\rho}\tilde{u}^2 + \bar{p} + \frac{2}{3}\bar{\rho}k \\ \bar{\rho}\tilde{u}\tilde{v} \\ \bar{\rho}\tilde{u}\tilde{w} \\ \tilde{u}(\bar{E} + \bar{p} + \frac{2}{3}\bar{\rho}k) \\ \bar{\rho}\widetilde{u_i''u_j''} \\ \bar{\rho}\tilde{u}\tilde{\epsilon} \end{pmatrix}, F_2 = \begin{pmatrix} 0 \\ \bar{\rho}\widetilde{u''u''} - \frac{2}{3}\bar{\rho}k \\ \bar{\rho}\widetilde{u''v''} \\ \bar{\rho}\widetilde{u''w''} \\ \bar{\rho}\tilde{u}(\widetilde{u''u''} - \frac{2}{3}k) + \\ \bar{\rho}\tilde{v}\widetilde{u''v''} + \bar{\rho}\tilde{w}\widetilde{u''w''} \\ 0 \\ 0 \end{pmatrix} \tag{32}$$

The Jacobian of F_1 can be diagonalized as in the case of the $k-\epsilon$ model [19]. The effect of F_2 on a solution is small, and, consequently, F_2 is evaluated using the average of the values of the two neighbouring nodes. In this approach the Reynolds stresses are not rotated, instead $\hat{F}_2$ is calculated directly from Eq. (23)

$$\hat{F}_2 = \begin{pmatrix} 0 \\ n_x(\bar{\rho}\widetilde{u''u''} - \frac{2}{3}\bar{\rho}k) + n_y\,\bar{\rho}\widetilde{u''v''} + n_z\,\bar{\rho}\widetilde{u''w''} \\ n_x\,\bar{\rho}\widetilde{u''v''} + n_y(\bar{\rho}\widetilde{v''v''} - \frac{2}{3}\bar{\rho}k) + n_z\,\bar{\rho}\widetilde{v''w''} \\ n_x\,\bar{\rho}\widetilde{u''w''} + n_y\,\bar{\rho}\widetilde{v''w''} + n_z(\bar{\rho}\widetilde{w''w''} - \frac{2}{3}\bar{\rho}k) \\ \tilde{u}\hat{f}_{2,2} + \tilde{v}\hat{f}_{2,3} + \tilde{w}\hat{f}_{2,4} \\ 0 \\ 0 \end{pmatrix} \tag{33}$$

where $\hat{f}_{2,i}$ is i:th element of the vector $\hat{F}_2$.

The second method of diagonalization utilizes the production term P_{ij}. The production term is exact in RSM and it can be separated from the other source terms. When the Jacobian of the production term is added to the flux Jacobian, the eigenvalues and the eigenvectors can be found. Eigenvalues and eigenvectors are fairly complex in comparison with the isotropic diagonalization, but there is no need to use central differences for the Reynolds stresses in the momentum equations. The resulting eigenvalues, i.e. the characteristic speeds, are

$$\begin{aligned} \lambda^{(i)} \;=\; & u, u+c, u-\sqrt{\widetilde{u''u''}}, u-\sqrt{\widetilde{u''u''}}, u+c, \\ & u, u+\sqrt{\widetilde{u''u''}}, u+\sqrt{\widetilde{u''u''}}, u, u, u, u \end{aligned} \tag{34}$$

where c is the speed of sound. For an arbitrary equation of state, the speed of sound is

$$c^2 \;=\; p_e\,p/\rho^2 + p_\rho + 3\widetilde{u''u''} \tag{35}$$

Notations p_e and p_ρ are

$$p_e \;=\; \frac{\partial p}{\partial e}|_\rho \quad p_\rho \;=\; \frac{\partial p}{\partial \rho}|_e \tag{36}$$

The Jacobian matrix, characteristic variables and the right eigenvector matrix are fairly complex and can be found in [15].

3.3 Boundary Conditions

The boundary conditions are given in the ghost cells on the block boundaries. The boundary condition types are given in [14]. At the free-stream boundary the values of the dependent variables are kept as constants. At the solid wall the velocity components are set to zero. In the present cases the wall is also assumed to be adiabatic. All turbulent quantities are set to zero, also $\hat{\epsilon}$. Because of this, these variables within the ghost cells are set to be of the opposite sign to the values in the cell adjacent to the surface. The ghost cell values are applied for the calculation of the flux adjacent to the surface. For the calculation of surface fluxes a second-order extrapolation is applied for the evaluation of the wall pressure and one-sided formulae are used for the derivatives at the wall.

Velocities at the symmetry boundaries can be calculated by first rotating the velocity components (u_1,u_2,u_3) into the local Cartesian coordinate system $(\hat{x}_1,\hat{x}_2,\hat{x}_3)$ that has a coordinate direction normal to the boundary face. The sign of the velocity component in this direction is changed and the three velocity components are then rotated back into the original (x_1,x_2,x_3) coordinate system. The resulting equation can be written as

$$U_{mir} \;=\; M\,U \tag{37}$$

The velocity vector U_{mir} is put into the ghost cells. This formulation for the velocity components has also been applied by Batina [1].

In general, the symmetry conditions of the stress tensor are very complicated formulations. After some manipulations it can be shown that the symmetry condition for the Reynolds stresses can be cast into the form

$$I_{mir} \;=\; M\,I\,M \tag{38}$$

which is applied as the velocity boundary condition of Eq. (37). Matrix M can be found after some calculation

$$M = \begin{pmatrix} 1-2n_x^2 & -2n_xn_y & -2n_xn_z \\ -2n_xn_y & 1-2n_y^2 & -2n_yn_z \\ -2n_xn_z & -2n_yn_z & 1-2n_z^2 \end{pmatrix} \tag{39}$$

where vector $(n_x,n_y,n_z)^T$ is the normal vector of the symmetry plane.

3.4 Time Integration Method

The discretized equations are integrated in time by applying the *DDADI*-factorization [12]. This is based on the approximate factorization and on the splitting of the Jacobians of the flux terms. In the implicit stage the factorization is done isotropicly. The implicit stage consists of a backward and forward sweep in every coordinate direction. The sweeps are based on a first-order upwind differencing. The boundary conditions are treated explicitly, and a spatially varying time step is utilized. The Jacobian matrices are approximated as

$$A^\pm \;=\; R(|\Lambda^\pm| + kI)R^{-1} \tag{40}$$

where $\Lambda^\pm$ are diagonal matrices containing the positive and negative eigenvalues, and k is a factor to ensure the stability of the viscous term. In order to estimate the value of k, the turbulent viscosity μ_T is evaluated from the calculated Reynolds stresses and dissipation.

The linearization of the source term is factored out of and performed before the spatial sweeps. Since the Jacobian matrix resulting from the the source term linearization of the Reynolds stress equations is prohibitively complex, it is approximated as

$$D \;=\; \frac{\partial Q}{\partial U} \;\approx\; -\frac{Q}{|\Delta U_{\max}|} \tag{41}$$

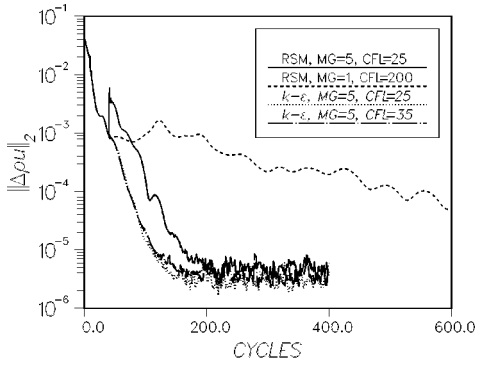

Figure 1. Comparision of the convergence history of the L_2-norm of the x-momentum residuals between different multigrid levels and different turbulence models.

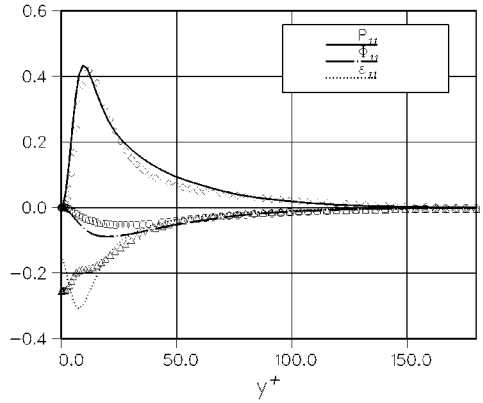

Figure 2. Comparision of the Reynolds-stress budgets between DNS data and the present calculation in a plane channel.

In this way, the maximum change of U caused by Q is limited to $|\Delta U_{\max}|$. The value of $|\Delta U_{\max}|$ is evaluated using the current values of $\bar{\rho}\widetilde{u_i'' u_j''}$ as

$$|\Delta(\bar{\rho}\widetilde{u_i'' u_j''})_{\max}| = C_{k,1}\left|\bar{\rho}\widetilde{u_i'' u_j''}\right| + C_{k,2}(1-\delta_{ij})\frac{2}{3}\bar{\rho}k \quad (42)$$

where $C_{k,1}$ and $C_{k,2}$ were set to 0.2 and 0.1 after test calculations. The second term in Eq. (42) assures a possible change of sign in the tangential components of Reynolds stresses.

A multigrid method is used to accelerate the convergence. The method of Jameson [7] with a simple V-cycle is applied. The implementation for the multigrid cycling is described in [20] and [19]. In order to enhance the stability of the multigrid cycling, the size of the correction $\Delta(\bar{\rho}\widetilde{u_i'' u_j''})$ from a coarse to a finer grid level is recalculated using the current value of $\bar{\rho}\widetilde{u_i'' u_j''}$ as

$$\Delta(\bar{\rho}\widetilde{u_i'' u_j''}) = \frac{\Delta(\bar{\rho}\widetilde{u_i'' u_j''})}{1+\dfrac{|\Delta(\bar{\rho}\widetilde{u_i'' u_j''})|}{C_1|\bar{\rho}\widetilde{u_i'' u_j''}| + C_2|\Delta(\bar{\rho}\widetilde{u_i'' u_j''})|}} \quad (43)$$

After test calculations C_1 and C_2 were set to 0.1 and 1.0. Variable C_2 assures a possible change of sign in the tangential components of Reynolds stresses.

4 TEST CALCULATIONS

In the first test case the SSG model is used for a fully developed flow in a plane channel [8]. The mesh is rectangular 48×32. The height of the first row of cells is Δy=0.005δ corresponding to $\Delta y^+ \approx 0.9$. Only half of the channel is modeled. The length of the computational mesh is 32δ. After having a converged result, the solution was taken from the downstream boundary and utilized as the upstream boundary condition of the next run. Fully developed flow was obtained after 4 computations, which corresponds to the length of 64 channel widths. The convergence of the results was checked by using a two-times denser grid. The results obtained with the two grid densities are practically identical.

Convergence of the L_2-norm of the x-momentum residuals can be seen in a Fig. 1 using different turbulence models and different numbers of multigrid levels. In all cases the first 50 cycles were calculated by using the $k-\epsilon$ turbulence model. As can be seen in Fig. 1, multigrid acceleration has a significant effect on the convergence rate. With 5 multigrid levels a converged result was obtained after 200 iteration cycles and with a single grid 1,800 iteration cycles were required. An iteration cycle using the RSM with the isotropic diagonalization was roughly 2 times slower than with the $k-\epsilon$ model. In this case also the difference in the convergence rate between the two diagonalization methods and the $k-\epsilon$ model is marginal, whereas the effect of the multigrid acceleration is significant.

Distributions of some source terms are presented in Fig. 2. Close to the wall the calculation did not agree with DNS [13] but away from the wall a good agreement was obtained.

As a second case Shima's model is applied for a flow in a curved duct [9]. The duct shown in Fig. 3 has two straight parts and a curved section. The rectangular cross-section of the channel has a width of H=20.3cm and a height of $6 \times H$. Only half of the channel is modeled. The Reynolds number based on the free-stream velocity is 224,000. The grid has a size of $64 \times 48 \times 128$. The height of the first row of cells is Δy=$4 \cdot 10^{-5}$ or $1.5 < \Delta y^+ < 3.5$.

Inlet conditions at x= $-$ 4.5H (x=0.0 is at the beginning of the curved section) are taken from the experiments. Pressure is given and the other variables are extrapolated at the outlet at a distance of 28.5H after the end of the curved section. The calculations were initiated on the third grid level. On the denser grid levels the calculation was started using the Reynolds-stress model directly, and the initial condition was

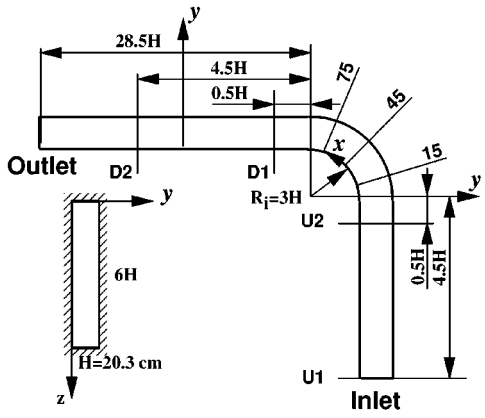

Figure 3. Geometry and measurement stations of the curved duct.

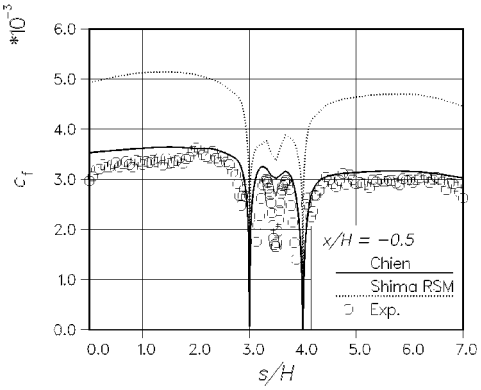

Figure 4. Friction coefficient along the channel wall at station U2.

taken from the result of the previous grid level. Because of stability reasons only two multigrid levels could be applied.

The friction coefficient is presented in Fig. 4 at station $U2$ ($x = -0.5H$). As can be seen, the friction is over-estimated. A similar result is obtained for every station. Calculated streamwise velocity distributions are presented in Fig. 5 at stations $U2$, 15, 45, 75, $D1$ and $D2$, and the corresponding distributions for the kinetic energy of turbulence in Fig. 6.

5 CONCLUSIONS

In this paper the implementation of the Reynolds-stress model in the existing Navier-Stokes solver has been described. Shima's model and the low-Reynolds number version of the Speziale, Sarkar and Gatski model have been applied. The solution algorithm is based on an approximate Riemann solver both in

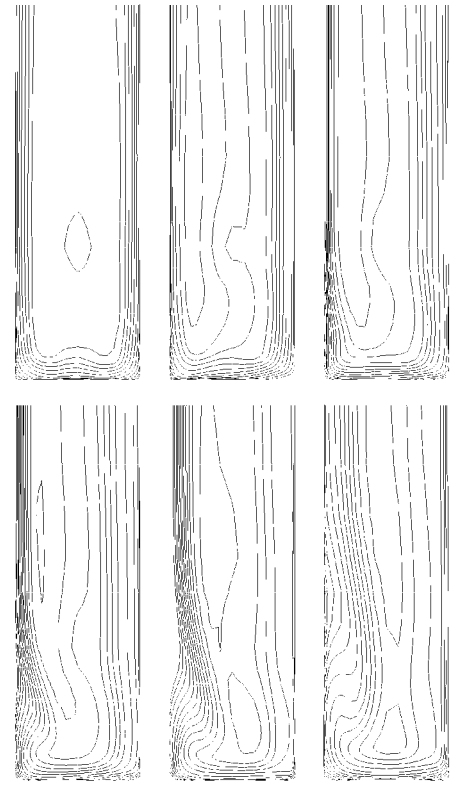

Figure 5. Streamwise mean velocity at different stations.

compressible and incompressible cases. Steady state is obtained via a time integration with a multigrid acceleration of convergence.

The coding has been simplified by the use of the Cartesian form of the equations. This has been accomplished by applying suitable rotation operators. These are utilized in the evaluation of fluxes as well as in the calculation of boundary conditions.

The developed numerical scheme appears to be stable and efficient. Per iteration cycle the calculation with the Reynolds-stress model takes only about twice as long as the calculation with Chien's low-Reynolds number $k - \epsilon$ model. Using a multigrid only a few hundred iteration cycles were required for the solution of a flow in a channel. Almost a comparable efficiency was obtained for a flow in a curved duct.

The approximate Riemann solution was done in two different ways. In the first approach the main flow equations are diagonalized as in the case of the $k - \epsilon$ model, and the Reynolds stresses are solved from scalar transport equations. In the more complicated approach the production term is included in the diagonalization and the Reynolds stresses are

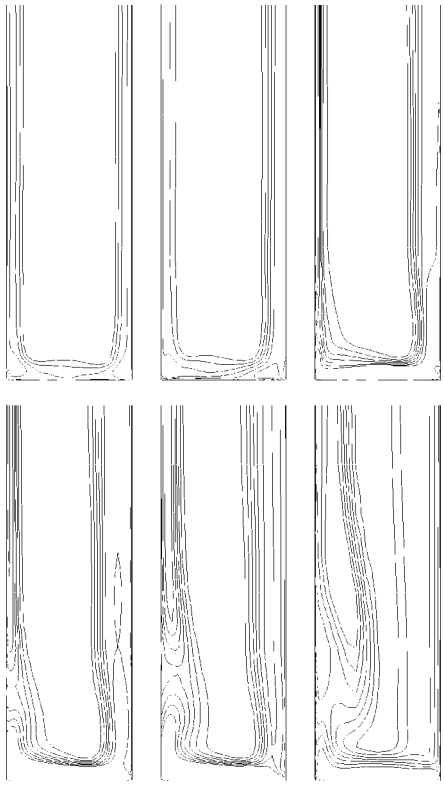

Figure 6. Kinectic energy of turbulence at different stations.

fully coupled with the flow equations.

The present test calculations are for incompressible flow. No significant differences in the results or performance obtained by the two methods was noticed. In the future the methods will be compared in more complex cases including supersonic flow.

REFERENCES

[1] J.T. Batina, 'Accuracy of an unstructured-grid upwind-euler algorithm for the ONERA M6 wing', *Journal of Aircraft*, **28**(6), 397–402, (June 1991).

[2] H.-C. Chen, 'Assessment of a Reynolds stress closure model for appendage-hull junction flows', *Journal of Fluids Engineering*, **117**(5), 557–563, (Dec 1995).

[3] Kuei-Yuan Chien, 'Predictions of channel and boundary-layer flows with a low-Reynods-number turbulence model', *AIAA Journal*, **20**(1), 33–38, (Jan 1982).

[4] A.J. Chorin, 'A numerical method for solving incompressible viscous flow problems', *Journal of Computational Physics*, **2**, 12–26, (1967).

[5] B.J. Daly and F.H. Harlow, 'Transport equations of turbulence', *Physics of Fluids*, **13**, 2634–2649, (1970).

[6] L. Davidson and A. Rizzi, 'Navier–Stokes stall predictions using an albebraic Reynolds-stress model', *Journal of Spacecraft and Rockets*, **29**(6), 794–800, (1992).

[7] A. Jameson and S. Yoon, 'Multigrid solution of the Euler equations using implicit schemes', *AIAA Journal*, **24**(11), (1986).

[8] J. Kim, P. Moin, and R. Moser, 'Turbulence statistics in fully developed channel flow at low Reynolds number', *Journal of Fluid Mechanics*, **177**, 133–166, (1987).

[9] W.J. Kim and V.C. Patel, 'Origin and decay of longitudinal vortices in developing flow in a curved rectangular duct', *Journal of Fluid Engineerin*, **116**, 45–52, (1993).

[10] B. E. Launder, G. J. Reece, and W. Rodi, 'Progress in the development of a Reynolds-stress turbulence closure', *Journal of Fluid Mechanics*, **68**, 537–566, (1975).

[11] F.S. Lien and M.A. Leschziner, 'A general non-orthogonal collocated finite volume algorithm for turbulent flow at all speeds incorporating second-moment turbulence-transport closure, part 1: Computational implementation', *Computer Methods in Applied Mechanics and Engineering*, **114**, 123–148, (1994).

[12] C.K. Lombard, J. Bardina, E. Venkatapathy, and J. Oliger, 'Multi-dimensional formulation of CSCM — an upwind flux difference eigenvector split method for the compressible Navier–Stokes equations', in *6th AIAA Computational Fluid Dynamics Conference*, pp. 649–664, Danvers, Massachusetts, (Jul 1983). AIAA Paper 83-1895-CP.

[13] N.N. Mansour, J. Kim, and P. Moin, 'Reynolds-stress and dissipation-rate budgets in a turbulent channel flow', *Journal of Fluid Mechanics*, **194**, 15–44, (1988).

[14] P. Rautaheimo, E. Salminen, and T. Siikonen, 'Parallelization of a multi-block Navier–Stokes solver', in *Proceedings of the ECCOMAS Congress*, Paris, (Sept. 1996).

[15] P.P. Rautaheimo and T. Siikonen, 'Numerical methods for coupling the Reynolds-averaged Navier–Stokes equations with the Reynolds-stress turbulence model', Report 81, Helsinki University of Technology, Laboratory of Applied Thermodymics, (1995). ISBN 951–22–2748–7.

[16] P.P. Rautaheimo, T. Siikonen, and A. Hellsten, 'Diagonalization of the Reynolds-averaged Navier–Stokes equations with the Reynolds-stress turbulence model', in *Proceedings of the IMACS-COST Congress*, Lausanne, (Sept. 1995).

[17] P.L. Roe, 'Approximate Riemann solvers, parameter vectors, and difference schemes', *Journal of Computational Physics*, **43**, 357–372, (1981).

[18] N. Shima, 'A Reynolds-stress model for near-wall and low-Reynolds-number regions', *Journal of Fluids Engineering*, **110**, 38–44, (1988).

[19] T. Siikonen, 'An application of Roe's flux-difference splitting for the $k - \epsilon$ turbulence model', *International Journal for Numerical Methods in Fluids*, **21**, 1017–1039, (1995).

[20] T. Siikonen, J. Hoffren, and S. Laine, 'A multigrid LU factorization scheme for the thin-layer Navier–Stokes equations', in *Proceedings of the 17th ICAS Congress*, pp. 2023–2034, Stockholm, (Sept. 1990). ICAS Paper 90-6.10.3.

[21] C.G. Speziale, S. Sarkar, and T.B. Gatski, 'Modelling the pressure-strain correlation of turbulence: and invariant dynamical systems approach', *Journal of Fluid Mechanics*, **227**, 245–272, (1991).

[22] D. Vandromme, 'Turbulence modeling for turbulent flows and implementation in Navier–Stokes solvers', in *Introduction to the Modeling of Turbulence*, von Karman Institute for Fluid Dynamics Lecture Series 1991-02, (1991).